*Clays and Clay Minerals*, Vol. 60, No. 5, 473–483, 2012.

# QUANTIFICATION OF HEMATITE AND GOETHITE CONCENTRATIONS IN KAOLIN USING DIFFUSE REFLECTANCE SPECTROSCOPY: A NEW APPROACH TO KUBELKA-MUNK THEORY

Ítalo Gomes Gonçalves*, Carlos Otávio Petter, and Jaqueline Lepkoski Machado

Laboratório de Processamento Mineral, Departamento de Engenharia de Minas, Universidade Federal do Rio Grande do Sul, Porto Alegre, Rio Grande do Sul, Brazil

**Abstract**—Kaolin ores are usually contaminated by some Fe-bearing minerals, the strong colors of which degrade the quality of the final product. A spectroscopic technique is sought to quantify the content of hematite and goethite, the main contaminant minerals in the kaolin from Capim River in Brazil, was the focus of this study. The total Fe content obtained through X-ray fluorescence showed a poor correlation with the brightness of kaolin, due to the inability to differentiate between the Fe contained in the (oxyhydr)oxides and the Fe present in the crystalline structure of kaolinite, especially when the Fe-bearing minerals occur in small quantities. Here, a new generic technique to quantify Fe (oxyhydr)oxides in kaolin, based on the Kubelka-Munk theory, is presented. A new interpretation of the theory was made that enables its use without the need to measure thin layers of material. The results with synthetic goethite and hematite were very positive ($R^2_{pred} \approx 0.99$) and experiments with contaminants from the mine are already underway.

**Key Words**—Brightness, Diffuse Reflectance, Goethite, Hematite, Kaolin, Kubelka-Munk Theory.

## INTRODUCTION

For most industrial minerals, color is associated directly with economic value. In terms of physics, the principal property that defines the term 'color' is the intensity of light reflected (or transmitted) by an object over the visible band, between 400 and 700 nm. This reflectance spectrum serves as the starting point for a variety of color-describing factors, the most common in the mineral industry being the brightness (TAPPI, 1977, 1986) and the L*a*b* system (HunterLab, 2008). Quality specifications for mineral products are usually based on these colorimetric parameters.

This market is becoming more selective and demanding in terms of the quality of raw materials and, alongside the traditionally controlled characteristics such as particle-size distribution and chemical composition, a trend now exists toward the establishment of increasingly stricter specifications for the optical properties of these materials. The new trend is occurring because most operations consuming these industrial minerals incorporate them into products in which the visual appearance is controlled. For these operations, which are mostly manufacturers of plastics, paper, paints, and ceramics, variations in the color of mineral materials result in difficulties in achieving the right color in the final product.

Strict specifications for colorimetric parameters such as whiteness and yellowness, as well as colorimetric coordinates such as L*, a*, and b*, are now being set. For the manufacturer of industrial minerals, the new specifications translate into problems simply because many of these parameters are alien to the tradition of the mining industry.

The main quality parameter in the kaolin industry is brightness, which is a weighted average of reflectance values over the range of 400−510 nm (TAPPI, 1977). Because of the lack of a better property, producers tend to also use brightness to assess the quality of the *in situ* ore and during the processing operations. Unprocessed kaolin is often accompanied by 'contaminant' minerals, however. For Brazilian kaolins, which are the object of the present study, the most notable contaminants are hematite ($Fe_2O_3$), goethite (FeOOH), and anatase ($TiO_2$).

Each of these contaminant minerals has a distinct color and each behaves differently during processing of the kaolin ore. Hematite and goethite, in particular, are particularly strong pigmenting agents and at concentrations as low as 100 ppm they can make the difference between a high-quality white pigment product for paper coating and waste material. As each Fe-bearing contaminant has a different color and responds differently to processing operations (*e.g.* magnetic separation, chemical bleaching, selective flocculation, and/or flotation in the case of kaolin), the *in situ* brightness tends to show a poor correlation with the brightness of the final product.

Brightness measurements are sometimes complemented with X-ray fluorescence (XRF) analysis of Fe and Ti, but the total oxide content provided by XRF is also poorly correlated with product quality because Fe may be in the form of goethite or hematite, or found within the crystalline structure of kaolinite. Thus, a more robust

* E-mail address of corresponding author:
italogoncalves@ibest.com.br
DOI: 10.1346/CCMN.2012.0600504

technique capable of distinguishing each mineral phase is desirable.

Diffuse reflectance spectroscopy (DRS) has been used to analyze iron (oxyhydr)oxide content both qualitatively (Torrent and Barrón, 2003; Liu *et al*., 2011) and quantitatively (Ji *et al*., 2002, 2006). These authors correlated slopes and inflection points at characteristic absorption bands with (oxyhydr)oxide content in natural soils.

Iron (oxyhydr)oxides are very common at the surface of Mars and their reflectance spectra spanning the ultraviolet−visible−near infrared range have been studied by several authors (Sherman *et al*., 1982; Morris *et al*., 1985; Sherman and Waite, 1985; Morris and Lauer, 1990; Bishop and Murad, 1996; Scheinost *et al*., 1998) for remote sensing and geologic characterization. These authors describe how the color of these minerals relates to their chemical composition and crystalline structure.

The approach presented here involves extensive use of the Kubelka-Munk (K-M) theory, which has been used for color matching (Schabbach *et al*., 2009 and 2011) and particle-size determination (Otsuka, 2004) in a simplified version. Unfortunately, the scattering constant, *S*, is very difficult to measure for dry powders, because the equations require a thin layer of material. Attempts have been made (Gonçalves and Petter, 2007; Gonçalves, 2009) but the experimental errors tend to be large.

The present study, therefore, aimed to develop a tool for the quantification of contaminant minerals in kaolin based on K-M theory without resorting to measurements of thin layers. Two techniques were tested: the one-constant simplified K-M theory, which uses information from one different wavelength per pigment in a mixture (Kortüm, 1969), and a new, two-constant approach, which takes into account differences in scattering between materials over the whole measured spectrum. Both techniques were tested with the same experimental dataset, which consisted of the reflectance spectra of mixtures between a bleached kaolin and synthetic Fe pigments.

## THEORY AND BACKGROUND

The following sections describe the spectral behavior of kaolin ore at Capim River, Brazil, its relation to the brightness-quality parameter, and how K-M theory can be used to determine mineral concentrations from reflectance spectra.

### *The reflectance spectrum and brightness*

The color of a kaolin sample is influenced directly by the optical properties of its most abundant minerals which are, in the case of the Capim River deposits, hematite, goethite, anatase, and kaolinite. The physical property that defines color is the reflectance spectrum in the visible region, regarded as being between 400 and 700 nm. Typical reflectance spectra of *in situ* kaolins (Figure 1) reveal that the sample color largely tends toward red or yellow (as reflectance increases with wavelength), with a few grayish (a somewhat flat curve) and purple samples (a slight decrease toward 550 nm, and then an increase).

The final kaolin product is needed to be as white as possible. One of the most common ways of quantifying whiteness is the ISO brightness measure (TAPPI, 1977), which is a weighted average of reflectance values in the 400−510 nm region (Figure 1). In the case of kaolin, mineral impurities have a significant impact on brightness, as they have greater absorption power in this region.

Brightness is a simple and efficient parameter for comparing different white mineral products. As a quality-control parameter, however, brightness is inefficient. Each contaminant has a different impact on a sample's color, and brightness cannot distinguish

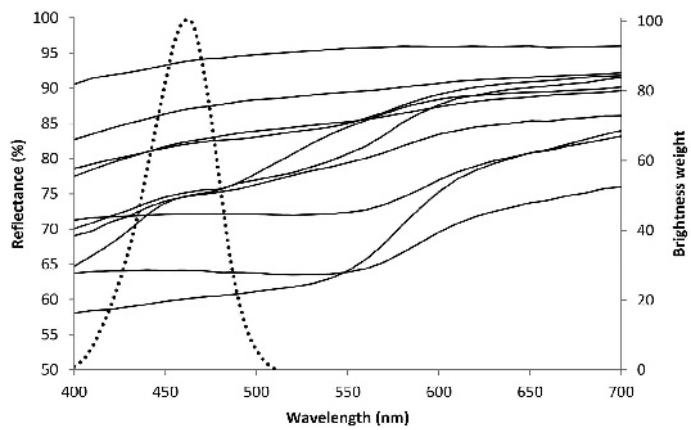


Figure 1. Typical reflectance spectra of Capim River deposits (full lines) and weights used to calculate brightness (dotted line). The weights favor the blue region of the spectrum (400−510 nm), where the contaminants absorb the most energy, hence the high sensitivity of the kaolin's brightness to contaminant content.

https://doi.org/10.1346/CCMN.2012.0600504 Published online by Cambridge University Press

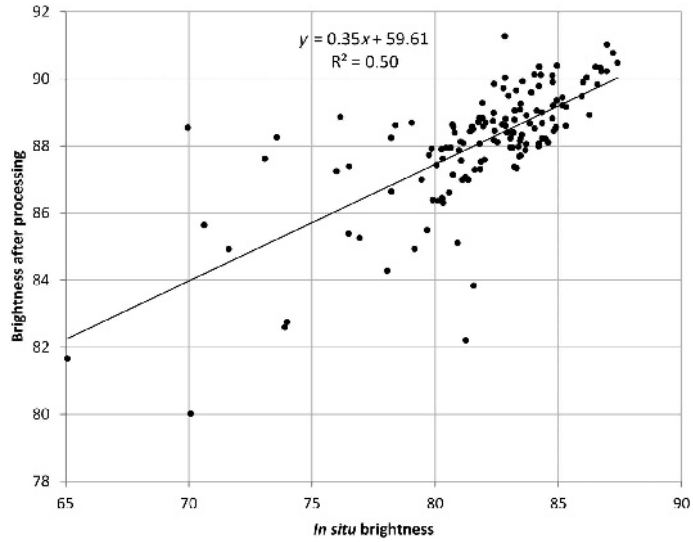


Figure 2. Scatterplot of brightness of the *in situ* material (after sieving to <44 μm) and after simulated processing in laboratory. The processing consisted of centrifugation (to control particle size), magnetic separation, and bleaching with sodium dithionite. The low correlation is due to variations in the proportions between the contaminant minerals.

between them. Furthermore, each contaminant responds differently to the processing operations, resulting in a poor correlation between the brightness of the *in situ* material and the final product (Figure 2). The Fe and Ti contents measured using XRF are sometimes used as a complement to brightness measurements, but they also fail to accurately assess a sample's quality (Figure 3). Although XRF itself is a very accurate technique, it is not capable of distinguishing between the structural Fe and the Fe contained in (oxyhydr)oxides. For samples with high brightness, the structural Fe content can be greater than the Fe contained in the contaminants. A highly absorptive contaminant at a concentration with the same order of magnitude of detection limit of XRF (usually 0.01–0.05%) can have a great impact on a sample's brightness. Because of factors such as particle size, aggregation of particles, element substitution, *etc.*, two samples with the same Fe and Ti concentrations may have very different reflectance spectra.

The reflectance spectra and brightness of samples treated with the pigments studied (Figure 4) revealed that the color of the mixture proved to be very sensitive to the pigments, especially hematite, even at low concentrations. This highlights the need for a technique capable of identifying each colorant's concentration instead of the bulk-element contents.

### *The Kubelka-Munk theory*

The K-M theory is largely used in industries such as paper (the biggest consumer of kaolin from Capim

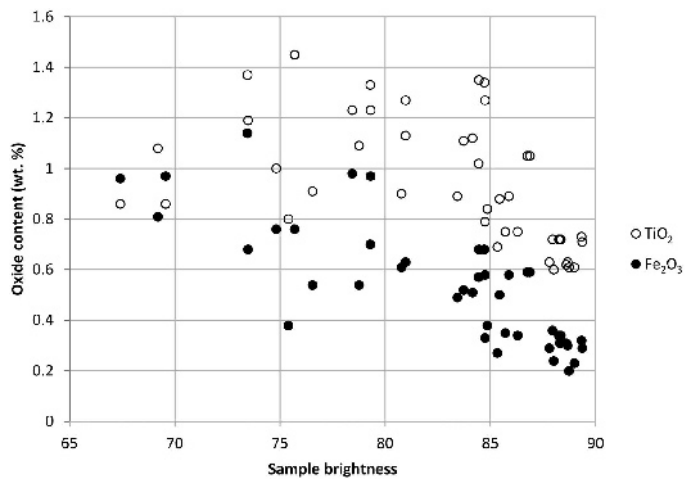


Figure 3. Scatterplot of sample brightness *vs.* Fe and Ti contents determined by XRF. Although the data show a general trend, factors such as variability of contaminant content, particle size, and structural Fe prevent the establishment of a useful correlation.

https://doi.org/10.1346/CCMN.2012.0600504 Published online by Cambridge University Press

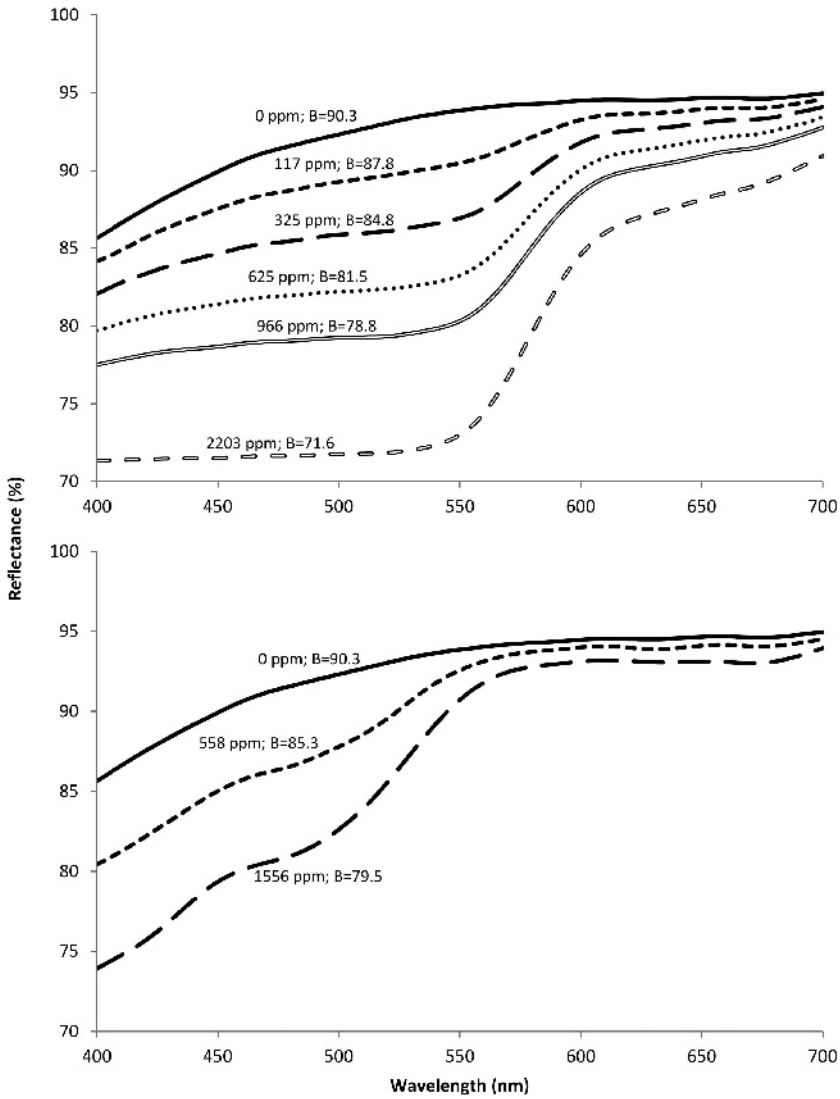


Figure 4. Reflectance spectra of binary mixtures of kaolin with hematite (upper) and goethite (lower). The concentration of pigment and the resulting brightness (B) are displayed alongside each curve. The greater the concentration, the more the resulting curve resembles that of the pure pigment.

River), paint, and textile where color is an important property. Equations 1 and 2 were described by Kortüm (1969) in his compilation of the deductions of Kubelka and Munk:

$$F = \frac{K}{S} = \frac{(1 - R_\infty)^2}{2R_\infty} \quad (1)$$

$$Sd = \frac{1}{b}\coth^{-1}\frac{1 - aR_0}{bR_0} \quad (2)$$

where $K$ is the absorption coefficient per unit length, $S$ is the scattering coefficient per unit length, $R_\infty$ is the reflectance of an opaque layer, $R_0$ is the reflectance of a thin layer over a black background, $a = 0.5(1/R_\infty + R_\infty)$, $b = \sqrt{(a^2 - 1)}$, $d$ is the layer thickness, and $F$ is the value of the K-M remission function (which is dimensionless). Equation 1 is applicable in the opaque case (*i.e.* the layer is thick enough so that transmittance is null) and equation 2 works for a transparent thin layer. As $d \to \infty$, $R_0$ tends to $R_\infty$ and equation 2 tends to equation 1. Using both equations, one can calculate the constants $K$ and $S$ of a given material for a given wavelength, λ.

In some cases the preparation of a homogeneous thin layer of material and measurement of its thickness is difficult, especially so for dry powders. According to equation 2, the greater a given material's scattering, the thinner the layer must be so that $R_0$ and $R_\infty$ will have enough contrast to enable the calculation of constants with a good accuracy. Gonçalves (2009) managed to

https://doi.org/10.1346/CCMN.2012.0600504 Published online by Cambridge University Press

obtain kaolin layers 30–50 μm thick but homogeneity was not guaranteed, and those layers did not reproduce the conditions in which the kaolin is found during brightness measurements.

Kortüm (1969) proposed a simplification of the theory for these cases. In a mixture of pigments the value of $F$ is given by a weighted average of each pigment's $K$ and $S$, with the weights being their relative concentrations

$$F = \frac{\sum_{i=1}^{m} K_i c_i}{\sum_{i=1}^{m} S_i c_i} \quad (3)$$

Considering a white substratum with high scattering and colored pigments in low concentrations, the substratum's scattering is said to dominate the system, so equation 3 may be simplified to:

$$F = F_0 + \sum_{i=1}^{m} K_i c_i \quad (4)$$

where $F_0$ is $K/S$ of the substratum and $K_i$ and $c_i$ are the absorption coefficient and concentration of pigment $i$, respectively. Mixing each pigment at a time with the substratum at different concentrations enables the calculation of each $K_i$ (Figures 5, 6). When measuring reflectance at a number of wavelengths equal to the number of pigments, solving a system of equations to calculate each $c_i$ is possible.

Unfortunately, the concentration of (oxyhydr)oxides in kaolin reaches values beyond the validity range of this simplification (Figure 7). For hematite, the validity threshold was ~1 wt.%. Also, if the substratum changes, the constants $K_i$ are no longer valid (Petter, 1994; Gonçalves and Petter, 2007). In practice the kaolin's reflectance is expected to change from one point of the deposit to another, and also during the processing operations, due to different particle-size distributions.

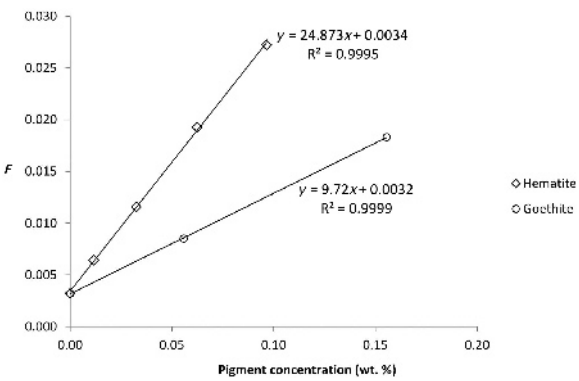


Figure 5. $F$ values obtained for low pigment concentrations at 500 nm (equation 1). According to the simplified K-M theory, the line slope is the absorption power of each pigment at this wavelength.

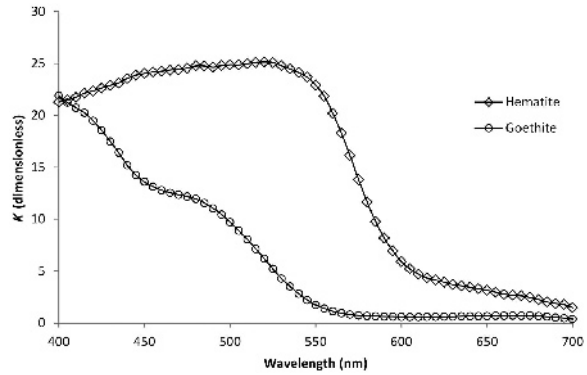


Figure 6. Pigments' absorption spectra used by the simplified K-M theory. Each dot corresponds to the line slope of a plot of $F$ *vs.* pigment concentration. The pigments have a greater absorption power in the 400–550 nm region (the violet–green region), which translates into greater reflectance in the yellow and red regions (550–700 nm).

Thus, a new methodology is necessary in order to deal with kaolin and its contaminants using the full K-M theory, but also avoiding the experimental errors associated with thin layers of powdered materials.

*The new approach*

The formulation described below is based on the opaque case only, and is generic enough to be tested in other applications of the K-M theory.

*Scattering ratio*. Consider equation 3, in the special case of a binary mixture between a reference material (R), usually but not necessarily a white substratum, and a material of interest (M) at a given wavelength:

$$F = \frac{K_R c_R + K_M c_M}{S_R c_R + S_M c_M} \quad (5)$$

$c_R + c_M = 1$, so equation 5 may be written in terms of $c_M$:

$$F = \frac{K_R + (K_M - K_R) c_M}{S_R + (S_M - S_R) c_M} \quad (6)$$

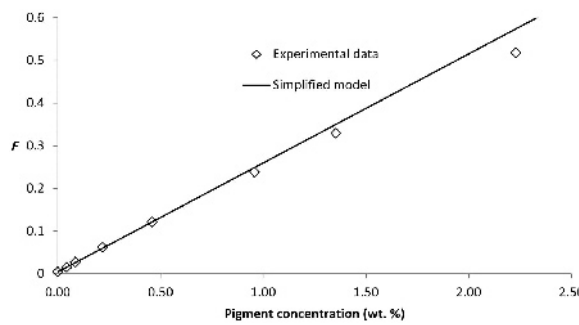


Figure 7. Comparison between experimental data points and the simplified K-M model for hematite at 500 nm. The model consists of the line formed by the points with concentrations <0.5 wt. %. Beyond that, the phenomenon starts to deviate from linearity.

https://doi.org/10.1346/CCMN.2012.0600504 Published online by Cambridge University Press

Taking the first derivative with respect to $c_M$, one finds

$$\frac{\partial F}{\partial c_M} = \frac{K_M S_R - K_R S_M}{[S_R + (S_M - S_R)c_M]^2} \quad (7)$$

Using the derivative to apply the linear approximation to equation 6 at the point where $c_M = 0$, one obtains

$$F = \frac{K_R}{S_R} + \frac{K_M S_R - K_R S_M}{S_R^2} c_M \quad (8)$$

The simplified theory's dependence on the substratum, as the line slope (previously considered to be simply the pigment's absorption; Figure 5) actually depends on both $K$ and $S$ of the pigment and the substratum, is explained in equation 8. Taking this line slope (denoted by $F'$) along with equation 1, one finds:

$$\frac{S_M}{S_R} = \frac{F'}{F_M - F_R} = \alpha_{MR} \quad (9)$$

The ratio $S_M/S_R$ is defined as the 'scattering ratio' of the material of interest over the reference, or $\alpha_{MR}$. Unlike the constants $K$ and $S$, the scattering ratio is measured easily, because it depends on $F_M$ and $F_R$ only (obtained through the reflectance of each material in a pure state), and $F'$, which is obtained experimentally (measuring the reflectance of mixtures with low concentrations, similarly to the simplified theory). The scattering ratio also has the following properties:

$$\begin{aligned} \alpha_{ij} &= \frac{1}{\alpha_{ji}} \\ \alpha_{ik} &= \alpha_{ij}\alpha_{jk} \\ \alpha_{ii} &= 1 \end{aligned} \quad (10)$$

with $i$, $j$, and $k$ being different kinds of pigments.

*Connection-line method*. Sometimes measuring directly the value of $F_M$ is impossible, due to the unavailability of a pure sample or experimental difficulties. Samples with very low reflectance tend to produce large photometric errors when applying equation 1 (as $R_\infty$ and $F$ are inversely proportional). For these cases, the following methodology is proposed.

Using equations 1 and 9, equation 6 may be written in terms of the scattering ratio:

$$F = \frac{F + (\alpha_{MR}F_M - F_R)c_M}{1 + (\alpha_{MR} - 1)c_M} \quad (11)$$

Note that the constant $S_R$ is canceled out. This function will have a positive concavity if $\alpha_{MR} < 1$, a negative concavity if $\alpha_{MR} > 1$, and will be a straight line if $\alpha_{MR} = 1$. Let $L$ be defined as the slope of the line connecting any point in the equation above with the reference point $(0, F_R)$ (Figure 8):

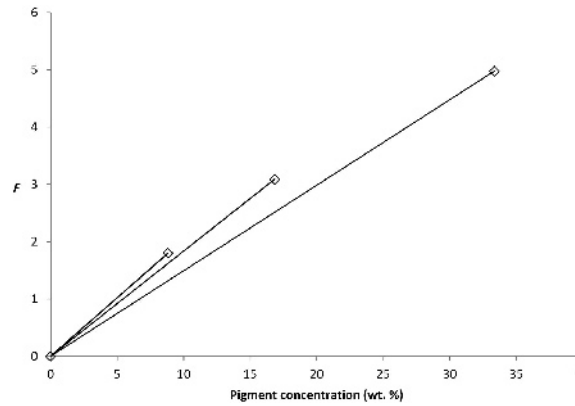


Figure 8. Experimental data points obtained for mixtures between kaolin and hematite at 500 nm. Each point is connected to the reference point $(0, F_R)$ through a line with a different slope (equation 12).

$$L = \frac{F - F_R}{c_M} \quad (12)$$

$L$ has the value $F_M - F_R$ when $c_M = 1$ and tends to $F'$ when $c_M \to 0$. Using equations 9, 11, and 12 one obtains:

$$\frac{1}{L} = \frac{1}{F'} + \frac{(\alpha_{MR} - 1)c_M}{F'} \quad (13)$$

This equation is of the type $y = a_0 + a_1 x$. Fitting a line to the values of $L$ calculated from the experimental data yields the coefficients $a_0$ and $a_1$. The model's constants are given by

$$\alpha_{MR} = \frac{a_1}{a_0} + 1 \quad (14)$$

$$F_M = \frac{1}{a_0 + a_1} + F_R \quad (15)$$

The scattering ratio of the synthetic pigments was calculated using this methodology (Figure 9). One advantage of equation 13 is that it retains its linear behavior for any concentration.

*Determination of concentrations*. For a given wavelength, λ, consider the generic case of equation 11, a mixture of a base material (0) with any number of pigments (*1, 2, ... m*):

$$F = \frac{\alpha_{0R}F_0 + \sum_{i=1}^{m}(\alpha_{iR}F_i - F_0)c_i}{\alpha_{0R} + \sum_{i=1}^{m}(\alpha_{iR} - 1)c_i} \quad (16)$$

The base material does not necessarily have to be the same reference material used for calibration. In general, reflectance is measured over a range of $n$ wavelengths and $n > m$. Manipulating the equation above so that each $c_i$ appears only once yields the linear equation relating all constants with the measured $F$ for the $j^{th}$ wavelength:

https://doi.org/10.1346/CCMN.2012.0600504 Published online by Cambridge University Press

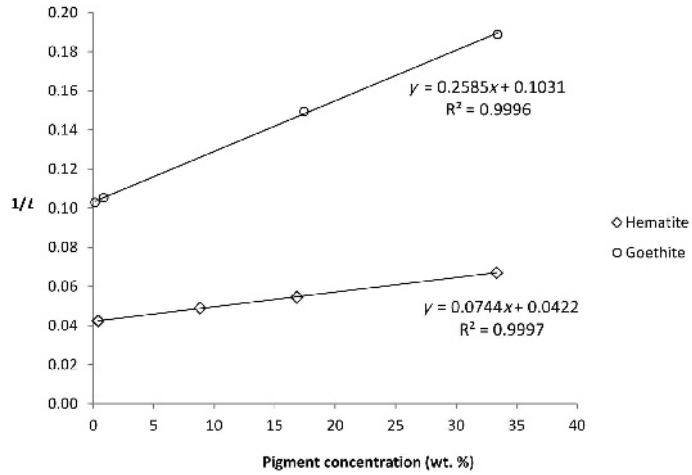


Figure 9. Connection line method for the estimation of constants at 500 nm. The equations fitted for each pigment correspond to equation 13. The values of $1/L$ are obtained through equation 12.

$$\sum_{i=1}^{m} \gamma_{ij} c_i = \gamma_{0j} \tag{17}$$

where

$$\gamma_{ij} = \alpha_{(iR)j}(F_{ij} - F_j) + \gamma_{0j}$$
$$\gamma_{0j} = \alpha_{(0R)j}(F_j - F_{0j})$$

One such equation exists for each measured wavelength. In matrix form this system has $n$ rows and $m$ columns:

$$\begin{bmatrix} \gamma_{11} & \gamma_{12} & \cdots & \gamma_{1m} \\ \gamma_{21} & \gamma_{22} & \cdots & \gamma_{2m} \\ \vdots & \vdots & \ddots & \vdots \\ \gamma_{n1} & \gamma_{n2} & \cdots & \gamma_{nm} \end{bmatrix} \begin{bmatrix} c_1 \\ c_2 \\ \vdots \\ c_m \end{bmatrix} = \begin{bmatrix} \gamma_{10} \\ \gamma_{20} \\ \vdots \\ \gamma_{n0} \end{bmatrix} \tag{18}$$

As $n > m$ for most cases, this system has more rows than columns. In order to use the whole spectral range measured, the least-squares method is employed:

$$\begin{bmatrix} \sum \gamma_{1j}^2 & \sum \gamma_{1j}\gamma_{2j} & \cdots & \sum \gamma_{1j}\gamma_{mj} \\ \sum \gamma_{2j}\gamma_{1j} & \sum \gamma_{2j}^2 & \cdots & \sum \gamma_{2j}\gamma_{mj} \\ \vdots & \vdots & \ddots & \vdots \\ \sum \gamma_{mj}\gamma_{1j} & \sum \gamma_{mj}\gamma_{2j} & \cdots & \sum \gamma_{mj}^2 \end{bmatrix} \begin{bmatrix} c_1 \\ c_2 \\ \vdots \\ c_m \end{bmatrix} = \begin{bmatrix} \sum \gamma_{1j}\gamma_{0j} \\ \sum \gamma_{2j}\gamma_{0j} \\ \vdots \\ \sum \gamma_{mj}\gamma_{0j} \end{bmatrix} \tag{19}$$

The solution to this system is the vector of concentration values which provides the best fit to the measured spectrum. When the experimental error in calibration and measurement is small, simple least squares provides a good solution. When the experimental error is large or when trying to match a spectrum containing pigments which are not part of the system, a

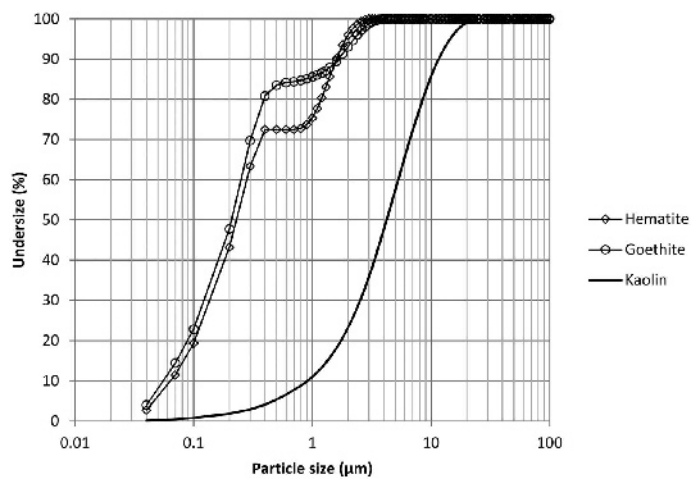


Figure 10. Particle-size distribution of the materials studied. The kaolin sample has a broad distribution, ranging from 20 to <1 µm. The synthetic pigments are much finer, with a narrower distribution.

https://doi.org/10.1346/CCMN.2012.0600504 Published online by Cambridge University Press

Table 1. Concentrations (ppm) of the binary mixtures between pigment and kaolin.

| Hematite | Goethite |
|---|---|
| 0 | 0 |
| 117 | 558 |
| 325 | 1556 |
| 625 | 8641 |
| 966 | 83471 |
| 2203 | 174379 |
| 4215 | 334171 |
| 88287 | |
| 168385 | |
| 333494 | |

non-negative least squares (NNLS) solution is necessary in order to avoid negative concentrations.

## MATERIALS AND METHODS

In order to test and exemplify the two techniques, a synthetic hematite ($d_{50}$ = 0.23 μm) and a synthetic goethite ($d_{50}$ = 0.21 μm) were mixed systematically with a white base. The white base consisted of a soft kaolin sample from the Capim River deposits ($d_{50}$ = 4.2 μm) which was processed in the laboratory in order to obtain a material with the greatest brightness possible (90.3 ISO). The processing consisted of magnetic separation and bleaching with sodium dithionite (3 kg/t, dry basis). Particle sizes were measured with a laser granulometer CILAS 1064 (CILAS, Orleans, France), with $d_{50}$ being the median of the particle-size distribution obtained (Figure 10). All reflectance measurements were performed using a Technidyne ColorTouch 2 spectrophotometer (Technidyne Corporation, New Albany, Indiana, USA) over the range of 400−700 nm with a 5 nm interval. Following the standard procedure for sample preparation in the kaolin industry (TAPPI, 1986), dry samples were pulverized for 30 s in a Technidyne Anglo pulverizer, which also served as a mixing instrument, and tablets of 40 mm diameter were then pressed manually (~250 KPa) and taken to the spectrophotometer.

Hematite and goethite were mixed separately with kaolin at different concentrations in order to calibrate the model (Table 1). Mixtures with low concentrations (<2000 ppm) were used to obtain the constants of the simplified K-M theory. The same data were used to calculate constants using the new approach, along with the more concentrated mixtures. Fifteen mixtures of both pigments in kaolin were also prepared in order to validate the formulation, in the range 0−25,000 ppm.

The results obtained were also used as examples to illustrate the application of the techniques presented. For the sake of simplicity, the examples either present a general spectral result or focus on the wavelength of 500 nm, where the two pigments have a good contrast.

## RESULTS AND DISCUSSION

Calibration results for the pigments studied (Figures 11−13) found that the new model fitted the data well, even for large concentrations, because it takes into account the non-linearity of the phenomenon. As both pigments are much finer than the kaolin, they are expected to have a scattering ratio >1. Hematite has greater scattering power in the red region of the spectrum, while goethite showed a somewhat more complex behavior. The estimated reflectance spectra were consistent with the pigments' colors (red for hematite, yellow for goethite), with the inflection points matching those found by other authors for natural (oxyhydr)oxides (Scheinost *et al*., 1998; Torrent and Barrón, 2003).

A slight difference exists between the calculated and measured reflectance spectra of the pigments (1−2%; data not shown) due to a different physical arrangement of the particles in the pressed tablet (degree of packing, covering of bigger particles by smaller ones, *etc*.). For low reflectance values, this difference has a great impact on the remission function, *F*, so the calculated values were chosen as the basis for this work, as the mixtures

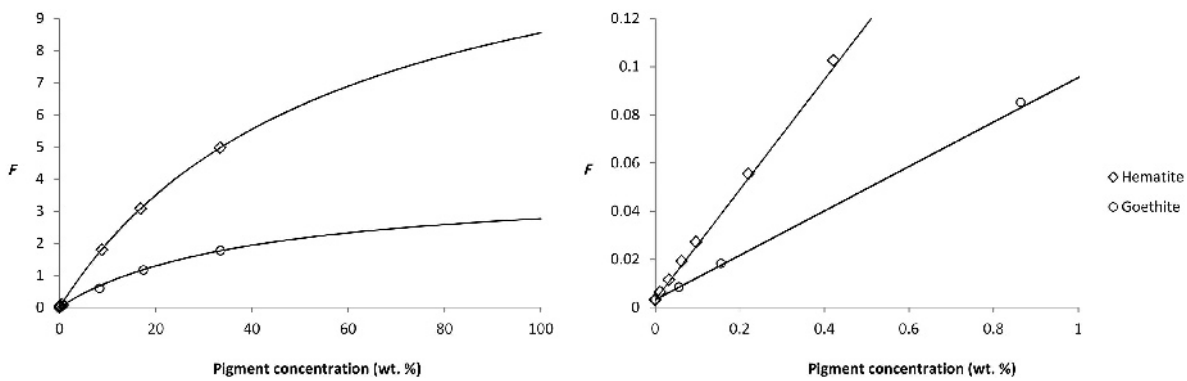


Figure 11. Model fit at 500 nm highlighting high (left) and low concentrations (right). The lines follow equation 11, using the constants α and *F* obtained for each pigment. The functions at 100% concentration correspond to the *F* values of the pure pigments.

https://doi.org/10.1346/CCMN.2012.0600504 Published online by Cambridge University Press

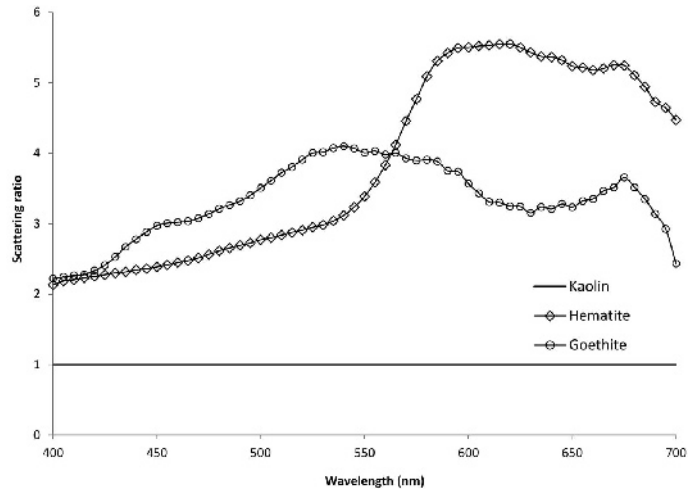


Figure 12. Scattering ratio of the materials studied relative to the kaolin. Hematite shows an increase in scattering toward the red region of the spectrum, while goethite has scattering peaks distributed throughout the visible range.

always have more kaolin than pigment and follow its general configuration.

Both the standard simplified model and the new methodology were validated, using 15 tertiary mixtures prepared in the range 0–25,000 ppm. The raw reflectance spectra for these tertiary mixtures (Figure 14) were transformed to $F$ (equation 1) and the concentrations of pigment were calculated. Following the new methodology, the calculations were performed using the simple least-squares method, which uses the whole spectral range from 400 to 700 nm (equation 19; NNLS gave the same results in this case). For the simplification, the reflectance values at 450 and 550 nm were chosen to form a linear system using equation 4 (this decision is somewhat arbitrary; in this case, 550 nm was chosen because of the great difference between the pigments' absorption constants and 450 nm was chosen due to goethite's distinct spectral behavior in this vicinity). Both models worked well, with a maximum absolute error of ~1800 ppm for the new model and 3000 ppm for the simplified model (Table 2). The model has shown good accuracy even for extremely small brightness values (35–50).

A threshold of 5000 ppm (0.5 wt. %) was stipulated in order to compare the two models for small and large concentrations. For small concentrations, the simplified model performed slightly better than the new model in the determination of hematite, but showed a much larger root mean square error (RMSE) for large concentrations (Table 3). For the determination of goethite, the new model performed slightly better over the whole range of concentrations tested.

The simplified model is expected to fail for large concentrations because it assumes a linear behavior for any concentration which, according to equations 6 and 11, is not true. The model deviates more quickly from linearity for hematite, which explains the greater error.

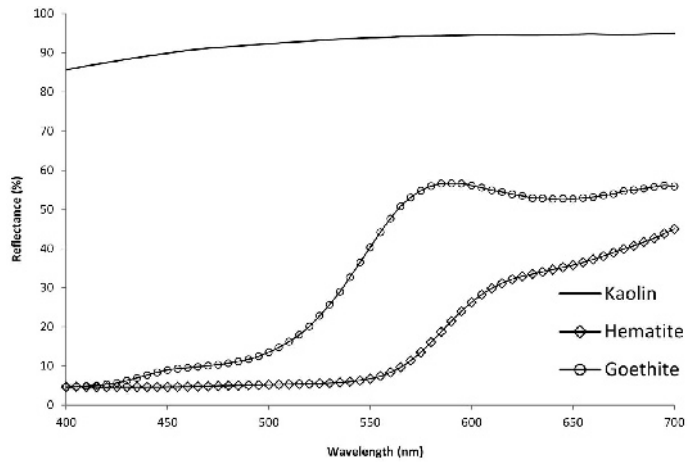


Figure 13. Reflectance spectra of the materials studied. The spectra of hematite and goethite were transformed back from the estimated $F$ values using equation 1.

https://doi.org/10.1346/CCMN.2012.0600504 Published online by Cambridge University Press

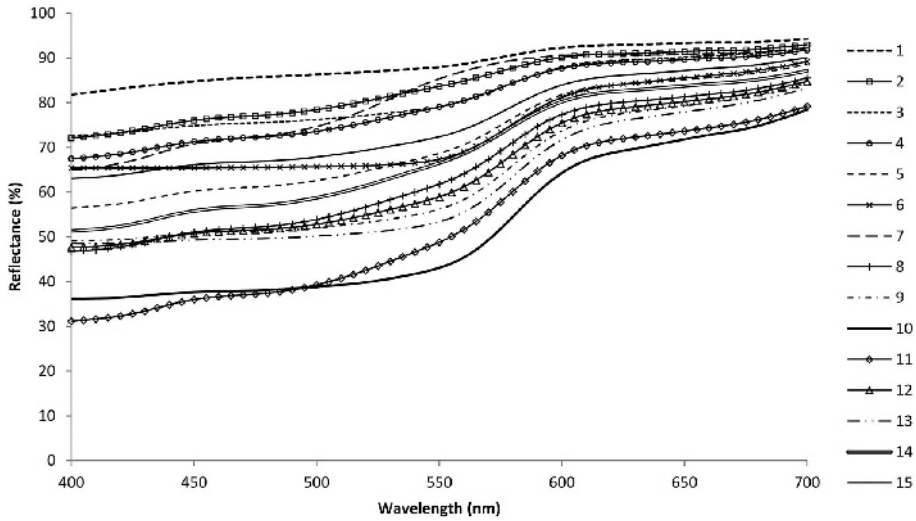


Figure 14. Reflectance spectra of the 15 mixtures between kaolin and the two pigments.

## CONCLUSIONS

Diffuse reflectance spectroscopy has shown the potential to be a quick, inexpensive, and accurate method for the determination of hematite and goethite concentrations in kaolin based on measurements of pressed tablets only, which is a common procedure in this industry. Unlike the more usual techniques, it allows the quantification of each mineral phase in small quantities, providing more information about the quality and 'processability' of the kaolin ore.

The new approach using K-M theory presented here has shown better results than the simplified theory, especially for (oxyhydr)oxide concentrations of >5000 ppm, which are very common in Capim River deposits. With the option of determining any (oxyhydr)-oxide concentration possible, this model may be used as an auxiliary tool for mine planning and process control without forcing the kaolin producer to rely on brightness measurements or XRF analysis alone.

In order to implement this technique in industrial practice, the actual contaminants from the mine must be studied, taking into account the variations in particle size.

When measuring in the opaque condition, the absolute constants $K$ and $S$ may be substituted by $F$ (easily measured or estimated) and the relative constant $\alpha$, thus avoiding measurements in the transparent condition.

The formulation presented is generic and usable in any application in which the original theory is valid.

Table 2. Comparison between the actual concentrations (ppm) of hematite and goethite and concentrations calculated through both models.

| | | Actual | | New approach | | Simplified K-M | |
|---|---|---|---|---|---|---|---|
| Mixture | Brightness | Hematite | Goethite | Hematite | Goethite | Hematite | Goethite |
| 1 | 85.0 | 233 | 108 | 277 | 113 | 262 | 132 |
| 2 | 76.2 | 516 | 1505 | 533 | 1439 | 497 | 1483 |
| 3 | 74.9 | 1023 | 765 | 1118 | 780 | 1054 | 830 |
| 4 | 71.4 | 972 | 2160 | 1026 | 2084 | 965 | 2127 |
| 5 | 60.3 | 2624 | 4163 | 2874 | 4426 | 2690 | 4475 |
| 6 | 65.5 | 3098 | 174 | 3561 | 249 | 3329 | 426 |
| 7 | 70.9 | 166 | 3553 | 198 | 3664 | 180 | 3699 |
| 8 | 51.1 | 4692 | 9155 | 4786 | 8989 | 4395 | 9025 |
| 9 | 50.8 | 8805 | 5585 | 7681 | 4334 | 7007 | 4738 |
| 10 | 37.7 | 18567 | 8907 | 17739 | 8876 | 15537 | 10157 |
| 11 | 36.1 | 11678 | 25155 | 11385 | 24551 | 9797 | 24026 |
| 12 | 50.8 | 7192 | 8766 | 6164 | 6941 | 5595 | 7230 |
| 13 | 49.4 | 9463 | 3069 | 9311 | 3201 | 8520 | 3677 |
| 14 | 55.9 | 3184 | 7077 | 3310 | 6982 | 3059 | 7020 |
| 15 | 66.1 | 1884 | 2100 | 2160 | 2346 | 2031 | 2388 |

https://doi.org/10.1346/CCMN.2012.0600504 Published online by Cambridge University Press

Table 3. Root mean square error of the two models for low and high concentrations (values in ppm).

| | New approach | | Simplified K-M | |
|---|---|---|---|---|
| | Hematite | Goethite | Hematite | Goethite |
| Under 5000 ppm | 198 | 139 | 136 | 267 |
| Over 5000 ppm | 789 | 940 | 1969 | 994 |
| Overall | 484 | 604 | 1142 | 662 |

Measurements in a broader spectrum (ultra-violet and infrared) may improve the accuracy of the technique.

## ACKNOWLEDGMENTS

The authors acknowledge CAPES (Coordenação de Aperfeiçoamento de Pessoal de Nível Superior) and Imerys Pigments for Paper and Packaging.

## REFERENCES

Bishop, J.L. and Murad, E. (1996) Schwertmannite in Mars? Spectroscopic analyses of schwertmannite, its relationship to other ferric minerals, and its possible presence in the surface material on Mars. Pp. 337–358 in: *Mineral Spectroscopy: A Tribute to Roger G. Burns* (M.D. Dyar, C. McCammon, and M.W. Schaefer, editors). Special Publication **5**, The Geochemical Society, St. Louis, Missouri, USA.

Gonçalves, I.G. (2009) Determinação da concentração de contaminantes no caolim através da teoria de Kubelka-Munk. MSc Dissertation, Universidade Federal do Rio Grande do Sul, Porto Alegre, Brazil, 68 pp.

Gonçalves, I.G. and Petter, C.O. (2007) Kubelka-Munk theory applied to industrial minerals: prediction of impurity content in kaolin. *Revista Escola de Minas*, **60**, 491–496.

HunterLab (2008) CIE L*a*b* color scale. *Insight on Color*, **8**, 4 pp.

Ji, J., Balsam, W., Chen, J., and Liu, L. (2002) Rapid and quantitative measurement of hematite and goethite in the Chinese loess-paleosol sequence by diffuse reflectance spectroscopy. *Clays and Clay Minerals*, **50**, 208–216.

Ji, J., Zhao, L., Balsam, W., Chen, J., Wu, T., and Liu, L. (2006) Detecting chlorite in the Chinese loess sequence by diffuse reflectance spectroscopy. *Clays and Clay Minerals*, **54**, 266–276.

Kortüm, G. (1969) *Reflectance Spectroscopy*. Springer-Verlag, Berlin.

Liu, Q.S., Torrent, J., Barrón, V., Duan, Q.Z., and Bloemendal, J. (2011) Quantification of hematite from the visible diffuse reflectance spectrum: effects of aluminium substitution and grain morphology. *Clay Minerals*, **46**, 137–147.

Morris, R.V. and Lauer, H.V. (1990) Matrix effects for reflectivity spectra of dispersed nanophase (superparamagnetic) hematite with application to Martian spectral data. *Journal of Geophysical Research*, **95**, 5101–5109.

Morris, R.V., Lauer, H.V., Lawson, C.A., Gibson, E.K., Nace, G.A., and Stewart, C. (1985) Spectral and other physicochemical properties of submicron powders of hematite ($\alpha$-$Fe_2O_3$), maghemite (g-$Fe_2O_3$), magnetite ($Fe_3O_4$), goethite ($\alpha$-FeOOH) and lepidocrocite ($\gamma$-FeOOH). *Journal of Geophysical Research*, **90**, 3126–3144.

Otsuka, M. (2004) Comparative particle size determination of phenacetin bulk powder by using Kubelka-Munk theory and principal component regression analysis based on near-infrared spectroscopy. *Powder Technology*, **141**, 244–250.

Petter, C.O. (1994) Contribution à l'etude de la valorisation de kaolins pour l'industrie papetiere: mise au point d'une methodologie colorimetrique, application à la selectivité miniere. PhD thesis, École des Mines de Paris, France.

Schabbach, L.M., Bondioli, F., Ferrari, A.M, Petter, C.O., and Fredel, M.C. (2009) Efficiency of Kubelka-Munk model in glazes with a black pigment and opacifier. *Journal of the European Ceramic Society*, **29**, 2685–2690.

Schabbach, L.M., Bondioli, F., and Fredel, M.C. (2011) Colouring of opaque ceramic glaze with zircon pigments: Formulation with simplified Kubelka-Munk model. *Journal of the European Ceramic Society*, **31**, 659–664.

Scheinost, A.C., Chavernas, A., Barrón, V., and Torrent, J. (1998) Use and limitations of second-derivative diffuse reflectance spectroscopy in the visible to near-infrared range to identify and quantify Fe oxide minerals in soils. *Clays and Clay Minerals*, **46**, 528–536.

Sherman, D.M. and Waite, T.D. (1985) Electronic spectra of $Fe^{3+}$ oxides and oxide hydroxides in the near IR to near UV. *American Mineralogist*, **70**, 1262–1269.

Sherman, D.M., Burns, R.G., and Burns, V.M. (1982) Spectral characteristics of the iron oxides with application to the Martian bright region mineralogy. *Journal of Geophysical Research*, **87**, 10169–10180.

TAPPI (1977) Brightness of pulp, paper and paperboard (directional reflectance at 457 nm). Technical standard.

TAPPI (1986) Brightness of clay and other mineral pigments (d/0 diffuse). Technical standard.

Torrent, J. and Barrón, V. (2003) The visible diffuse reflectance in relation to the color and crystal properties of hematite. *Clays and Clay Minerals*, **51**, 309–317.

(*Received 23 January 2012; revised 15 October 2012; Ms 647; AE; J. Stucki*)